CERN/LHCC 2000-027
Status Report RD-46

EUROPEAN ORGANIZATION FOR NUCLEAR RESEARCH

May, 2000

RD46 STATUS REPORT

High-resolution tracking devices based on capillaries filled with liquid scintillator

G. Bardelloni, D. San Segundo Bello, J.L. Visschers – NIKHEF, Amsterdam

M. R. Mondardini, K. Winter – Humboldt Universität zu Berlin

P. Annis, L. Benussi, V. Fanti, P. Vilain, G. Wilquet – IIHE ULB-VUB, Brussels

J.P. Fabre, J. Panman – CERN, Geneva

E.N. Kozarenko, I.E. Kreslo, V. Tyukov – JINR, Dubna

J. Goldberg – TECHNION, Haifa

A. Bay, C. Currat, P. Koppenburg – University of Lausanne

N. Bruski, D. Frekers, T. Wolff, H.J. Wörtche – Westfälische Wilhelms-Universität, Münster

N. D'Ambrosio, S. Buontempo, A. Ereditato – INFN Sezione di Napoli

A. Frenkel, F. Galeazzi, K. Harrison, B. Liberti, G. Martellotti, G. Penso – INFN Sezione di Roma and University "La Sapienza"

A.V. Ekimov, S.V. Golovkin, A.M. Gorin, V.N. Govorun, A.M. Medvedkov, V.G. Vasil'chenko – IHEP, Protvino

1 Introduction

The RD46 Collaboration was formed by bringing together experts in the fields of scintillators, scintillating-fibre tracking and optoelectronics, with the primary objective of developing high-resolution tracking detectors for HEP [1].

We have developed high-resolution tracking detectors based on glass micro-capillaries filled with organic liquid scintillator of high refractive index. Track images projected onto the readout end of a capillary bundle are visualized by an optoelectronic chain.

In addition, the Collaboration has widely investigated other possible fields of application for the optoelectronic technique of real-time high-resolution imaging.

Since the previous report [2] the work has mainly been devoted to:

- Development and study of the performance of a micro-vertex detector comprising thin planar layers of capillaries filled with liquid scintillator (see Appendix).

Significant effort has also been dedicated to:

- A review of the work done by the collaboration, in particular concerning the technique for producing large-size capillary bundles and the assessment of the performance attained [3].
- Further study of liquid scintillators [4, 5].
- Improvements in the technique of high-resolution photodetection using an Electron-Bombarded CCD vacuum tube (EBCCD) [6, 7].

In parallel with the above activities, the Collaboration has investigated different applications of the techniques developed. We mention in particular:

- Study of the EBCCD as a cost-effective multichannel readout for high-granularity tracking and calorimetry in large-scale experiments [7].
- Application of the EBCCD in industrial and biomedical radiography, in particular for mammography.

In this document we briefly discuss results obtained by the collaboration since the previous status report.

2 Capillary layers

The capillary technique has been investigated in collaboration with industrial companies: Schott[1], Geosphaera[2] and, more recently, Taper Vision[3]. The present capillary technology produces capillary bundles (packed arrays of capillaries) that are of a consistently high quality, and are hexagonal or square in cross-section. Uniform planar arrays, suitable for the construction of a low-density microvertex detector, have been built at CERN by assembling small-size square bundles, produced by TaperVision. The techniques of layer assembly, cutting and filling have been progressively refined and are now well established.

[1]Schott Fiber Optics Inc., Southbridge MA 01550-1960, USA.
[2]Geosphaera Research Centre, Moscow 117261, Russia
[3]TaperVision Inc., Pomfret, CT 06258, USA.

A prototype, consisting of three thin layers, each 2 mm thick, has been built. In the Appendix we give a detailed description of this detector and of the tests performed. The results show the high potential for pattern recognition offered by this detection technique: the high hit density gives the possibility to measure track vectors in a single detector station.

3 Liquid scintillators

Liquid scintillators (LS's) characterised by a high refractive index and emission in the green region have been tested. They are based on different solvents in combination with one of four dopants. Special purification techniques and the influence on the light yield of different gas atmospheres and temperature have been extensively studied. The results obtained were published in 1999 [4, 5].

Among other things, it has been shown that eliminating the air dissolved in LS's significantly increases the light yield. Nearly all of this enhancement is preserved if the LS's are kept in an inert atmosphere of Ar or Ne (Fig. 1).

In the temperature interval 20–60 °C, some LS's exhibit a light yield stability of ~ 3 % (better than that of NE102A plastic scintillator). This feature can be relevant in some applications, for example HEP calorimetry.

Light yields have been also measured for temperatures well below the scintillators' freezing points. Around the liquid-solid phase transition a peculiar behaviour, similar to that of liquid crystals, has been observed (Fig.2). At -120°C the light yield was found to be higher by a factor ~ 2 than that at room temperature. In the best case a light yield of 144 % of that of anthracene was obtained, a value much higher than that of any plastic scintillator.

4 Development of the EBCCD technique

The EBCCD, developed in collaboration with Geosphaera, is a high-resolution electrostatically focused image intensifier with a reversed, thinned CCD (silicon pixel array) in place of the usual phosphor screen. The high gain (of the order of 4000 electrons per photoelectron) and the low-noise front-end electronics, allow excellent single-photoelectron detection.

Our collaboration has continued the development of the EBCCD technique, with considerable progress since our previous status report:

- Further tests have been carried out with the EBCCD used as a single-photoelectron detector. Studies have been performed [7] of the single-photoelectron cluster size (Fig. 3), of the signal-to-noise separation (Fig. 4), gain uniformity (Fig. 5), and gain linearity vs. applied voltage.

- Different types of EBCCD tubes, with a range of photocathode diameters, have been designed and tested.

  A large Megapixel EBCCD tube (80 mm photocathode) has been constructed with a view to both radiographic applications and low-cost multichannel readout of large fibre detectors.

First prototypes of EBCCD tubes with GaAs photocathode have been produced and are under test. They have a spectral sensitivity in the red and near infrared region, extending the possible applications for the EBCCD.

- A new type of EBCCD camera was designed and produced. A compact power supply and a high-voltage gate are placed inside the camera housing. This allows to avoid HV cables and connectors outside the camera, improving the overall reliability. A Peltier cooling system is installed on the EBCCD input window, strongly reducing the photocathode's thermal emission. The EBCCD can then be operated with negligible noise in continuous readout cycles, without having a trigger acting on the tube's fast gate.

- A new, more stable low-noise front-end electronics, which performs parallel readout of the two CCD output registers (10 MHz clock, implying 100 ns/pixel or 50 ms/full image), has been designed. The 8-bit ADC on the frame grabber board has now been replaced by a 12-bit ADC on the front-end board. This reduces both the gain needed from the electronics for good single photoelectron detection and the total noise, and at the same time increases the dynamic range (relevant when single-photoelectron detection for tracking and calorimetric measurements have to be provided simultaneously).

5 EBCCD for radiography

We are investigating the use of the EBCCD for digital radiography in industrial (Fig. 6) and biomedical applications. In particular, we have developed a first prototype of a mammographic device based on the Megapixel EBCCD tube mentioned above. This has an 80 mm photocathode, a working area of 62×62 mm^2, and a demagnification factor of 4.6. The setup considered is shown schematically in Fig. 7.

X-rays convert and produce light in a thin ($\sim$ 100 μm) layer of high-density scintillator deposited on a fibre-optic plate coupled to the input window of the EBCCD. Only the photons emitted in the angular acceptance of the optical fibres are transmitted to the photocathode. The best results, in terms of detection quantum efficiency and resolution, have been obtained with LSO (Lu_2SiO_5) crystals. A spatial resolution of 10 lp/mm, at the surface of the converter, has been measured with 20 keV X-rays generated by a point-like source.

The final image is the superposition of several frames obtained in consecutive exposures. This permits to optimize the contrast, increasing the number of bits/pixel in the final image while avoiding the saturation of the pixel potential wells.

Compared with traditional mammography, based on a film screen, the EBCCD system has all the advantages of digital devices, such as instantaneous presentation, fast image processing, easier diagnosis, permanent electronic archiving and retrieval. Moreover, the test of the prototype with a standard mammographic phantom, simulating a 45-mm-thick compressed breast, demonstrated a much better contrast, making possible a strong reduction in the dose absorbed by the patient. Figure 8 shows the images of a nylon fibre, 1.56 mm in diameter, inside the phantom, as recorded using our EBCCD prototype, and as recorded by a high-quality film-screen mammography system, with a typical dose of $\sim$ 1 rad.

The input area of the present EBCCD detector is sufficiently large for this device to be used in many medical applications, including guided biopsy and localization of

suspicious lesions.

A large industrial effort is needed for the production of a full-scale mammographic device with an EBCCD tube having a sensitive area of 240×180 mm^2 and containing two CCD chips, each with 9×10^6 pixels.

6 EBCCD for multichannel fibre readout

6.1 Principle of the multichannel fibre readout

During the last year the RD46 collaboration has studied the EBCCD as a cost-effective multichannel readout for a high-granularity detector based on scintillators and wavelength shifting (WLS) fibres. Many fibres, from different scintillator elements, are grouped in an ordered bundle and connected to the input window of the EBCCD. This method is particularly attractive in experiments operating at a low event rate, for large dimension tracking and for calorimeters, where a huge number of WLS fibres must be read.

The EBCCD readout has important advantages over other devices usually used for this purpose, such as multichannel Photomultipliers (PMT's):

- The EBCCD has excellent single-photoelectron detection, with a nonuniformity (about 15%) much smaller than that of multichannel PMT's.
- The high spatial resolution of the EBCCD allows fibres packed tightly together to be read with negligible crosstalk.
- A very large number of fibres can be read by a single device, reducing costs and simplifying the setup. For a typical fibre diameter of 1 mm, the existing Megapixel EBCCD tubes, with a photocathode diameter of 40 mm or 80 mm, can read 525 or 4500 fibres.
- The Quantum Efficiency of the EBCCD tube is in the range of 10−14 %. Detection efficiency can be increased inexpensively by coupling the input fibre-optic window of the EBCCD tube to an additional image intensifier, with quantum efficiency optimized for the fibre emission spectrum.
- The cost of the EBCCD readout, including electronics and DAQ system, is about 14 \$/channel at 525 fibres/tube and a few \$/channel at 4500 fibres/tube. This is more than an order of magnitude cheaper than is possible with others types of readout.

6.2 Prototypes and test results

Together with physicists from other collaborations, we have performed, with a 15 GeV/c pion beam, a test of a prototype made of 54 plastic scintillator bars, assembled in layers. The scintillation light emitted by a bar was collected by a WLS fibre (1 mm in diameter) glued with optical epoxy at the centre of the bar.

The readout chain is shown schematically and in photographs in Fig. 9 and Fig. 10 respectively. In this chain the EBCCD is preceeded by a first-generation image intensifier having a high quantum efficiency ($\sim$ 20 %) and a demagnification of 1:0.65. This

image intensifier improves the sensitivity and permits readout of up to $\sim 10^3$ fibres with the one chain (cost/channel of less than 10 \$).

In Fig. 11 we show a schematic view of a layer of bars, and of the image of a m.i.p. crossing the best layer. The bars, produced by different methods (extrusion or injection moulding) were 30-75 cm long, with various cross-sections. They were made of polystyrene and doped with three combinations of dyes. The surface of a bar was coated with one of several materials: teflon, tyvec, tetratec, or aluminized mylar.

Three types of double cladding WLS fibres were used: POL-HI-TECH S248, KURARAY Y11, and BICRON BCF91A. The readout ends of the 54 fibres were placed at a centre-to-centre spacing of 1.2 mm and glued in an optical connector, plugged onto the EBCCD. The non-readout end of the fibres had no mirror.

Some of the results of the tests are reported in Table 1, for various scintillator bars and WLS fibres. The best result was obtained with bars made by extrusion that had a cross-section of 18×25 mm^2. They were coated with tyvec, and were read using Y11 fibres. A m.i.p., crossing 18 mm of scintillator, produced an average of 22.6 p.e. at a distance d=1.25 m from the photocathode and 12.9 p.e. at d=5.7 m. A light attenuation length of 7.7 m has been measured (Fig.12).

In Fig. 13 we also show results obtained with three cells made of extruded white polycarbonate profiles (inner cross-section of 9×8.5 mm^2 and length of 0.9 m) filled with the liquid scintillator EJ-399-01 and read by Y11 fibres of 1.2 mm diameter.

In another test (not reported in Table 1) a scintillator bar coupled with a BCF91A Bicron fibre was read with our EBCCD chain: the observed hit density was higher by a factor of ~ 2 compared to what was previously reported from a measurement made on the same bar with a 16-channel PMT HAMAMATSU R5900-M16. This is consistent with the higher QE of our first photocathode at the wavelength emitted by the fibres.

7 Conclusions

The RD46 Collaboration has undertaken a varied and productive programme, developing liquid scintillators, detectors based on glass capillaries, and various optoelectronic devices. The major achievements, since the previous status report, are the results attained with capillary layers and with the EBCCD, confirming their strong potential for a wide range of applications.

The work completed fulfills the engagements agreed in the past with the LHCC. Nevertheless, the Collaboration plans to continue its R&D programme at the home laboratories and at CERN. In particular, work will be devoted to further studies of liquid scintillators (including LS based on lquid crystals and cheap LS based on oil for large size detectors), and to developments connected with the use of the EBCCD in the applications discussed. We also envisage investigating the possibility of using the new high-resolution hybrid pixel detectors (under development for Alice, LHCb, medipix chips in DEP image intensifiers) for a fast parallel readout of the capillary-layer detector in a high-rate environment.

The RD46 collaboration would like to be officially recognized at Cern for the next two years and take advantage of the general CERN facilities. Financial support is ensured by National Agencies, and (mainly) by the European Union's TMR program "Micro-track Imaging", contract number ERBFMRX-CT98-0196, which recently passed the midterm review and will continue for two more years.

References

[1] R. van Dantzig et al. (RD46 Collaboration), "High resolution tracking devices based on capillaries filled with liquid scintillator", R&D Proposal CERN/LHCC 95-7, P60 / LDRB, 1995.

[2] RD46 Status Report CERN/LHCC 97-38

[3] P. Annis et al., preprint CERN-EP/99-132 (September 1999) to be published in Nucl. Instr. and Meth. A.

[4] S. Buontempo et al., Nucl. Instr. and Meth. **A 425** (1999) 492.

[5] G.I. Britvich et al., Nucl. Instr. and Meth. **A 425** (1999) 498.

[6] S. Buontempo et al., Nucl. Instr. and Meth. **A 413** (1998) 255.

[7] "A multichannel Single-Photon Sensitive Detector for HEP: the Megapixel EBCCD", Presented by L. Benussi at the Second International Conference on New Developments in Photon Detection, Beaune (France), 21-27 June 1999.

[8] A. Bay et al., "A high-resolution tracking hodoscope based on capillary layers filled with liquid scintillator", submitted to Nucl. Instr. and Meth. A.

Table 1: Light yields and attenuation lengths measured using different scintillator bars and WLS fibres.

Scintillator	Cross-section	Production Coating	WLS fiber	$N_{p.e.}$ d=2.7 m	$N_{p.e.}$ d=5.7 m	λ (m)
1.5% PTP + 0.01% POPOP	18 × 25 mm^2	extrusion Tyvec	Y11 1 mm	20.3	12.9	7.7
1.5% PTP + 0.01% POPOP	20 × 20 mm^2	moulding teflon	Y11 1 mm	7.1	4.8	7.7
1% PPO + 0.01% POPOP	20 × 20 mm^2	moulding teflon	BCF 1 mm	12.0		
1.5% PTP + 0.01% POPOP	20 × 20 mm^2	moulding teflon	S248 1 mm	5.1	0.8	3.2
1.5% PPO + 0.01% POPOP	20 × 20 mm^2	moulding teflon	Y11 1 mm	12.3	8.3	7.7
1.5% PTP + 0.01% POPOP	8.5 × 25 mm^2	extrusion Tyvec	Y11 1 mm	13.0	8.8	7.7
1% PTP + 0.01% POPOP	10 × 20 mm^2	moulding paint	BCF 1.2 mm	8.5 d=1.85 m		

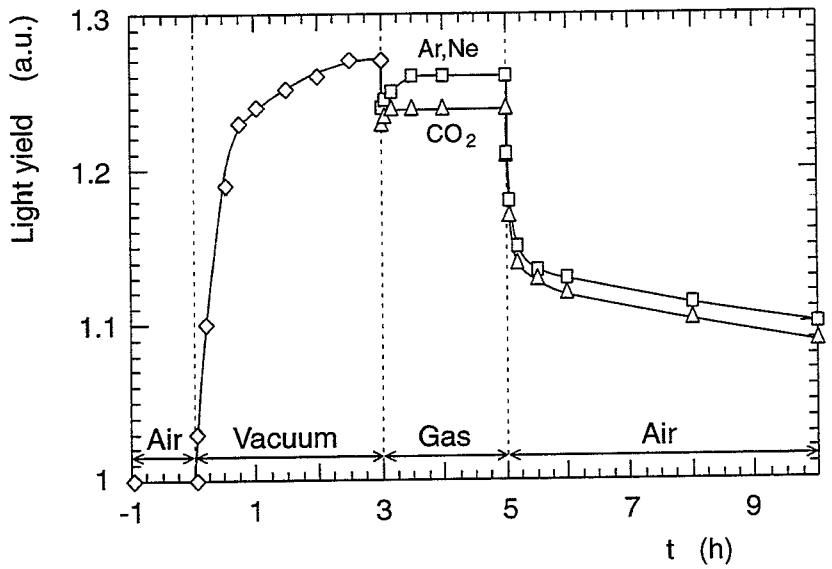

Figure 1: Variation with time, t, of the light yield of 1MN+R6 scintillator at 20 °C: when in air at normal pressure ($t < 0$ h); when degassed in vacuum ($0 < t < 3$ h); when placed in a gas atmosphere ($3 < t < 5$ h); and when contact with air is restored ($t > 5$ h). The curves refer to Ar and Ne gas (upper curve) and to CO_2 (lower curve). The light yield in air was normalized to 1. Similar curves were obtained for nitrogen and freon.

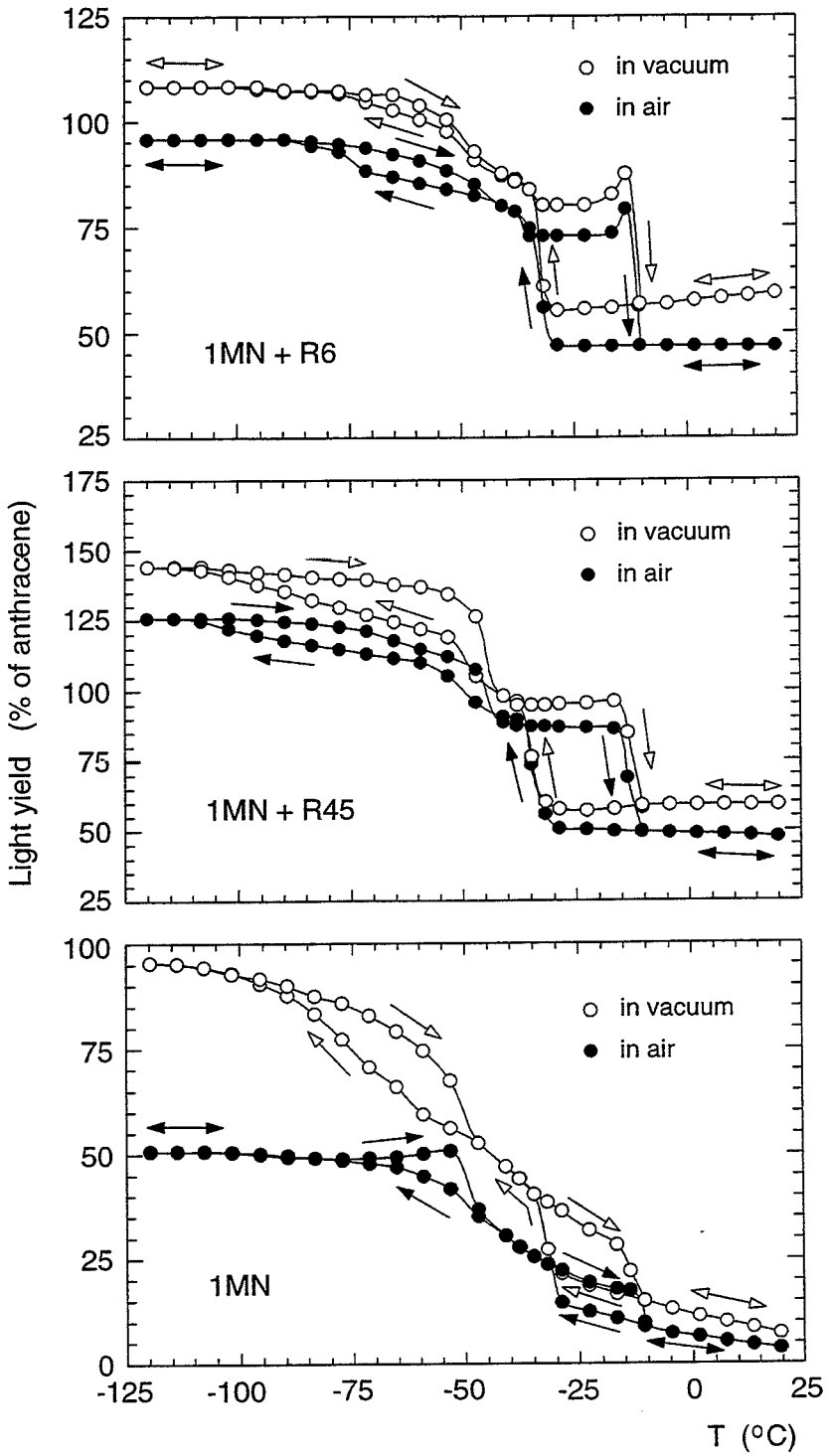

Figure 2: Light yield as a function of temperature for 1MN+R6 and 1MN+R45 scintillators and for pure 1MN solvent. Measurements were performed in air at normal pressure and in vacuum after a suitable degassing time. The arrows indicate the time sequence of the measurements during the cooling and heating processes.

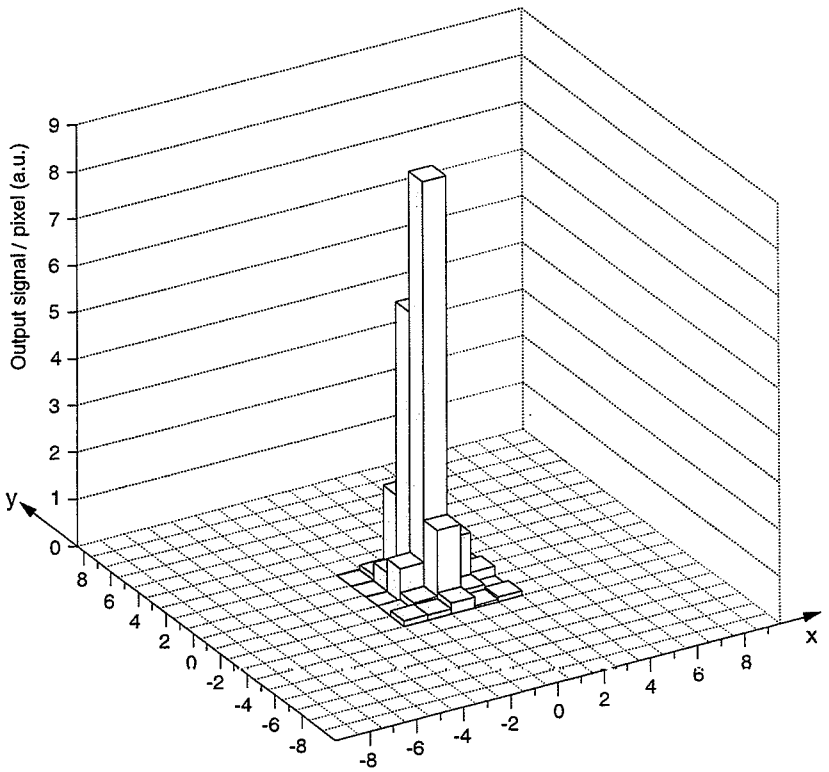

Figure 3: Average distribution, on the CCD plane, of the charge per pixel for a single photoelectron.

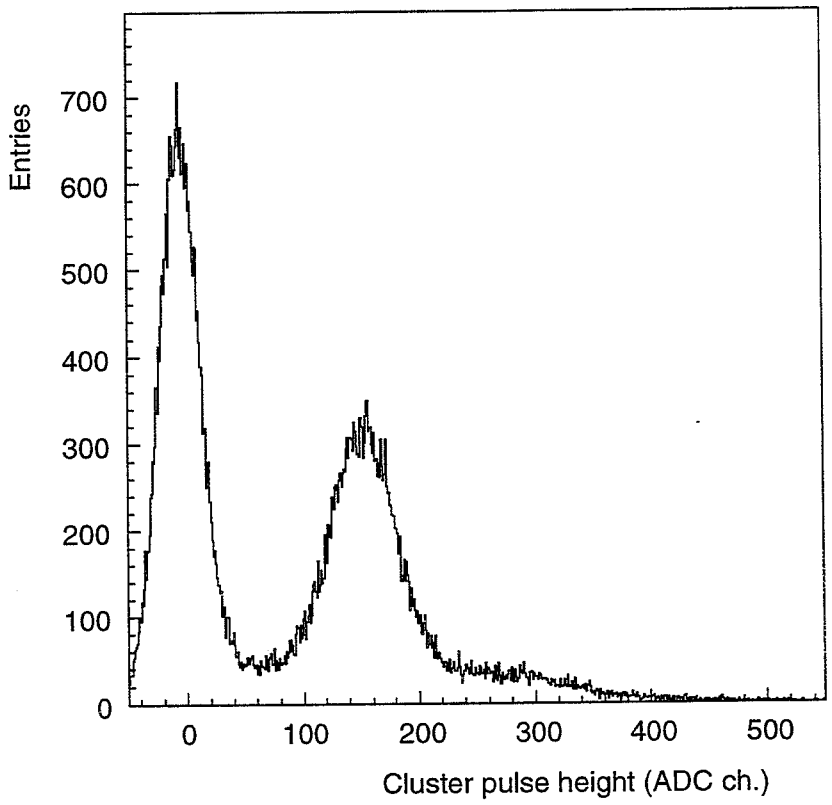

Figure 4: Cluster pulse height distribution. The single-photoelectron peak is clearly separated from the noise.

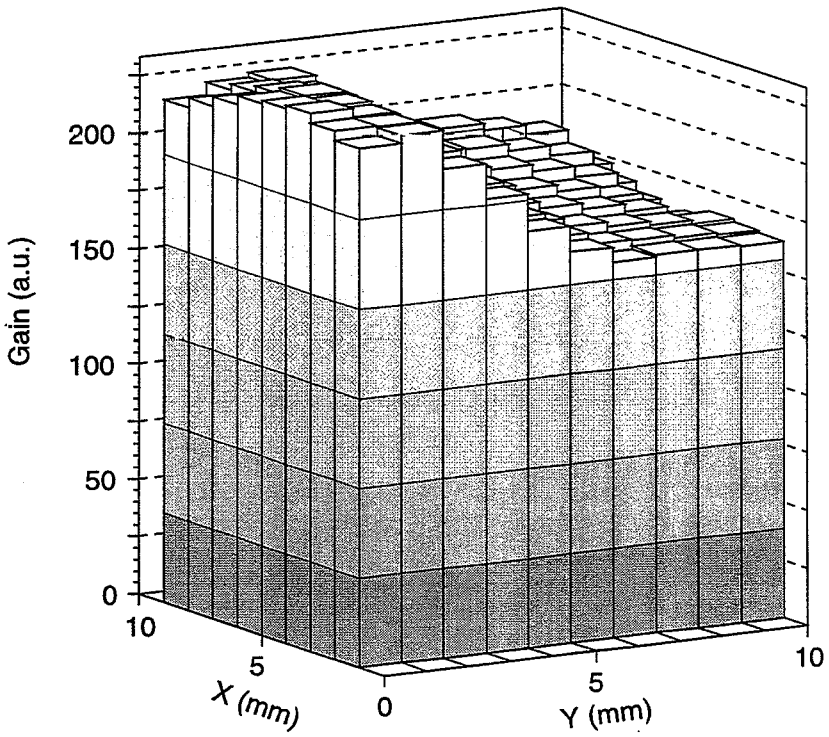

Figure 5: Map of the CCD gain.

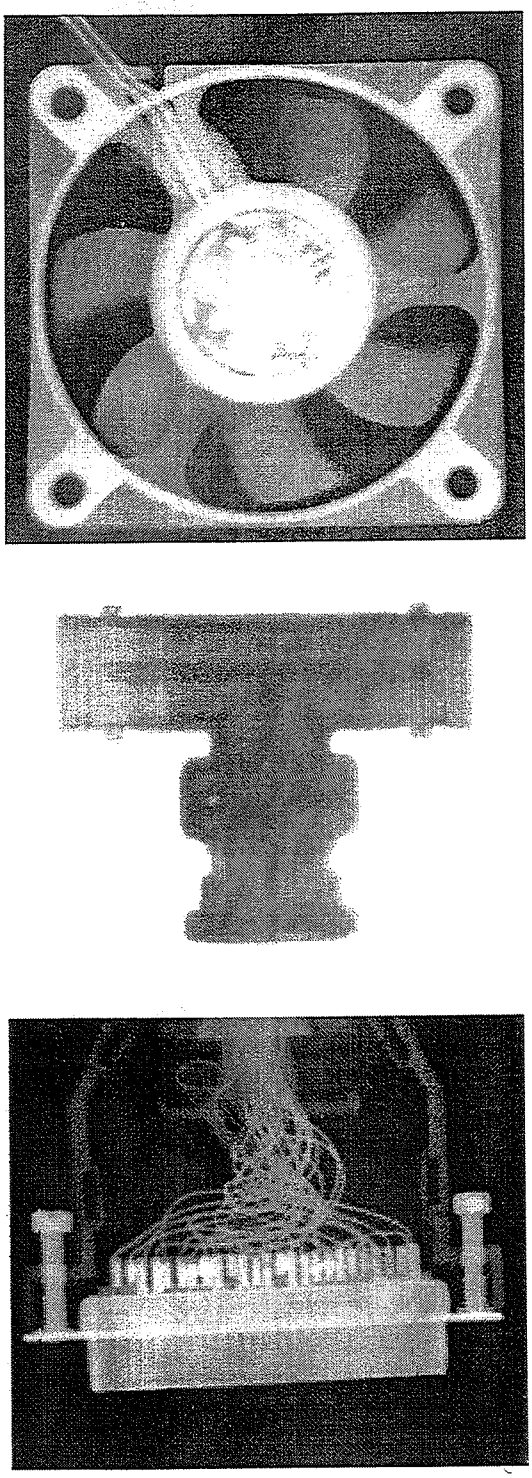

Figure 6: Examples of radiographic images recorded with the EBCCD: a CPU fan (top); a BNC connector (centre); a PC serial connector (bottom).

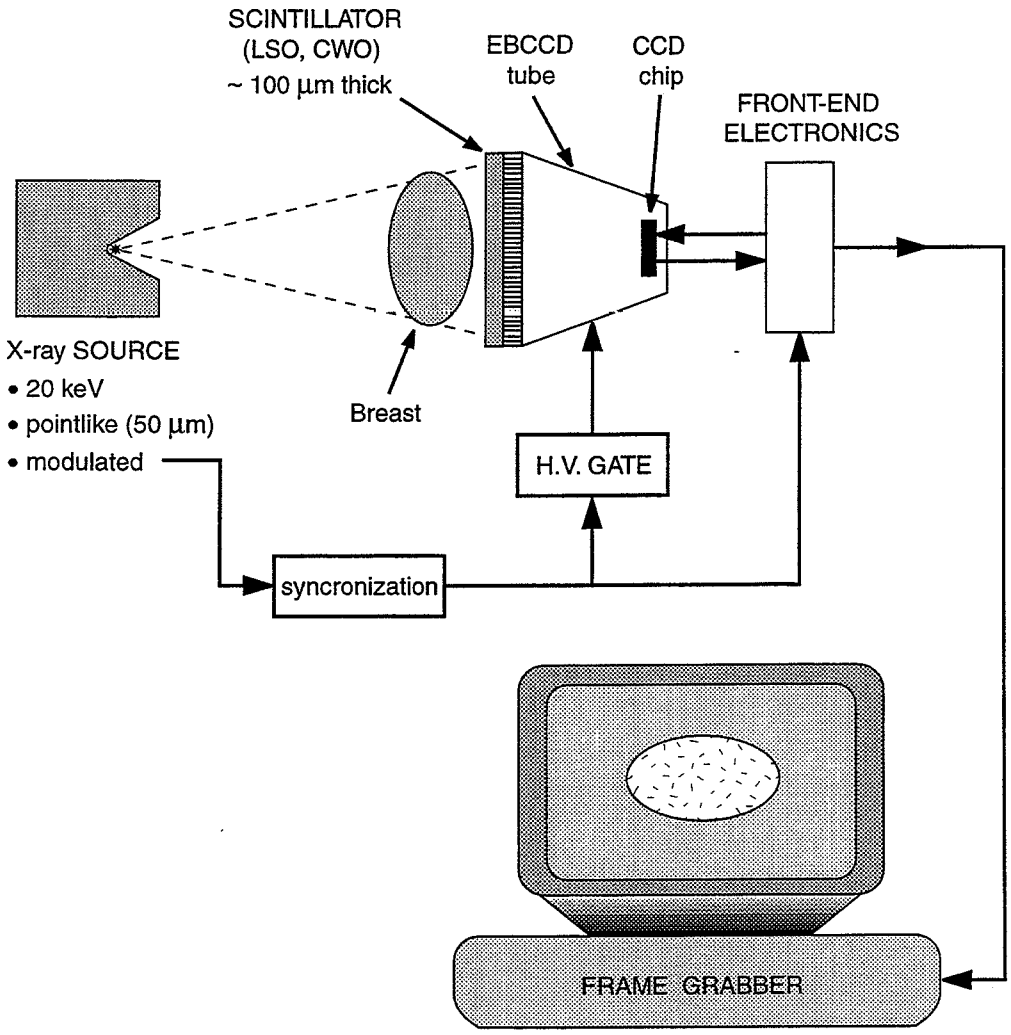

Figure 7: Scheme of the mammographic device.

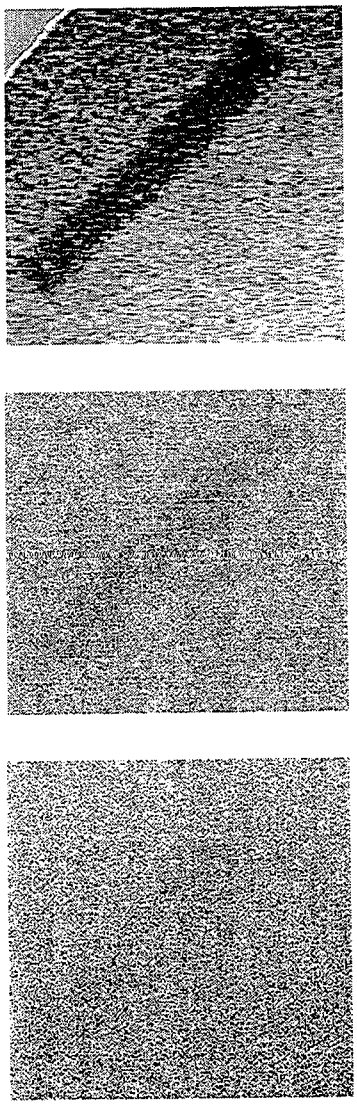

Figure 8: Images of a nylon fibre, 1.56 mm in diameter, in a standard mammographic phantom, using the EBCCD device (top) and using a good-quality film-screen system, with (centre) and without (bottom) an anti-scatter grid.

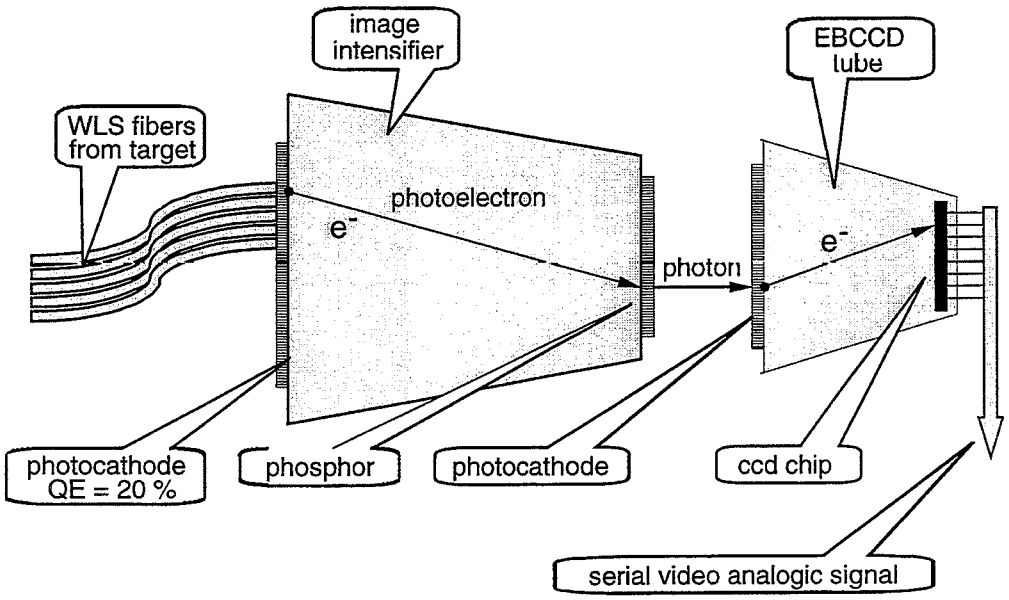

Figure 9: EBCCD readout configuration.

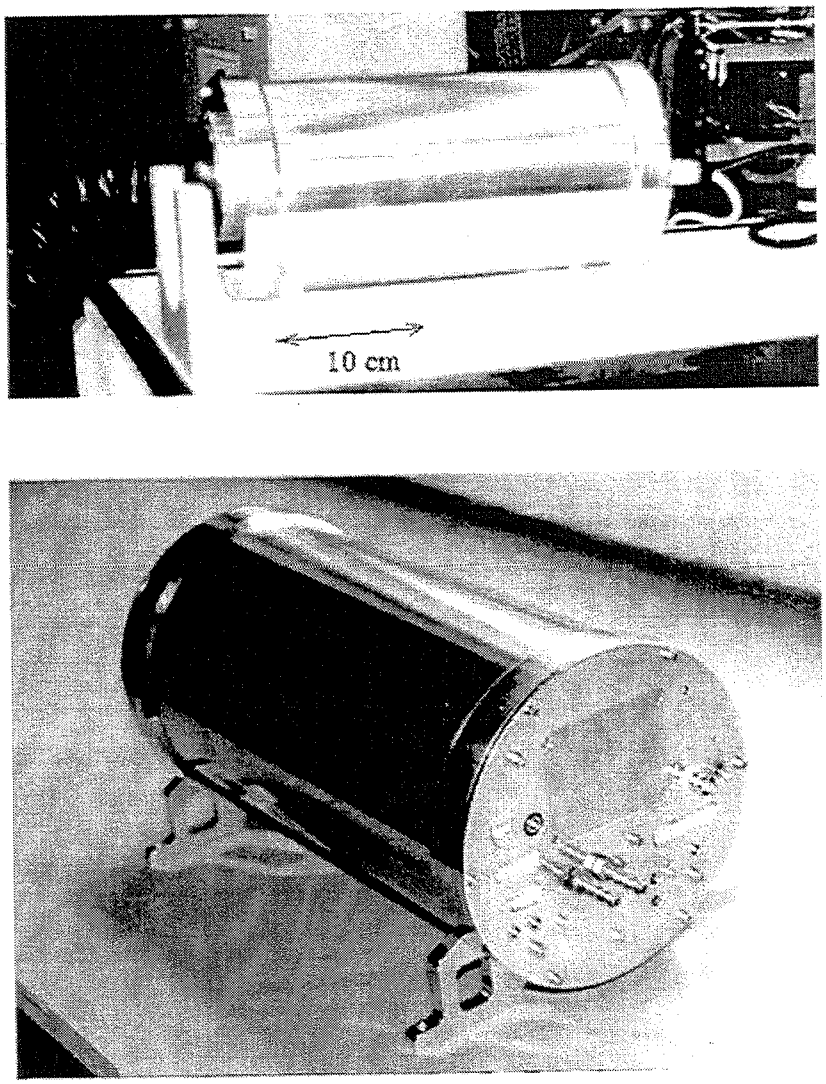

Figure 10: Photographs of the readout chain.

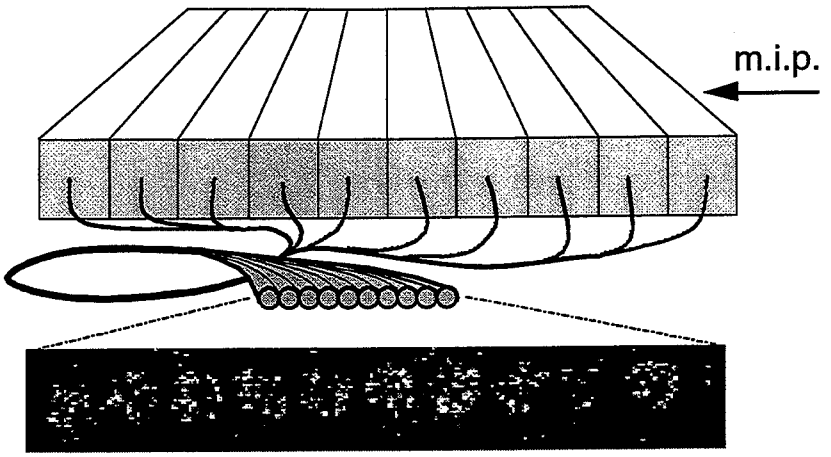

Figure 11: Schematic view of a layer of bars, and the image of a m.i.p. crossing the best layer composed of ten bars. Each of the bars has a cross-section of 18×25 mm^2. The spots are the signals of single photoelectrons.

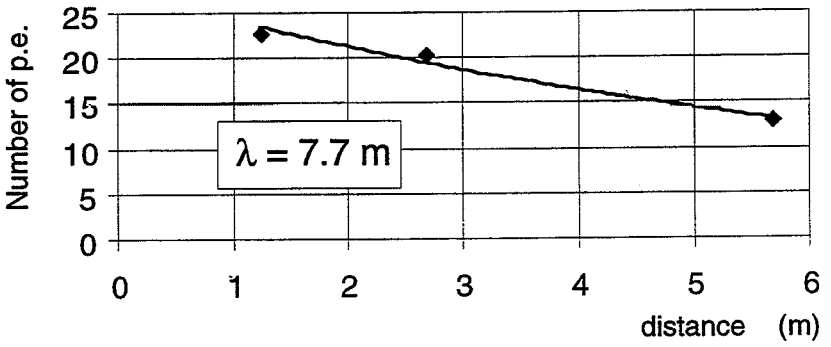

Figure 12: Number of photoelectrons vs. distance from photocathode for the 18×25 mm^2 bars.

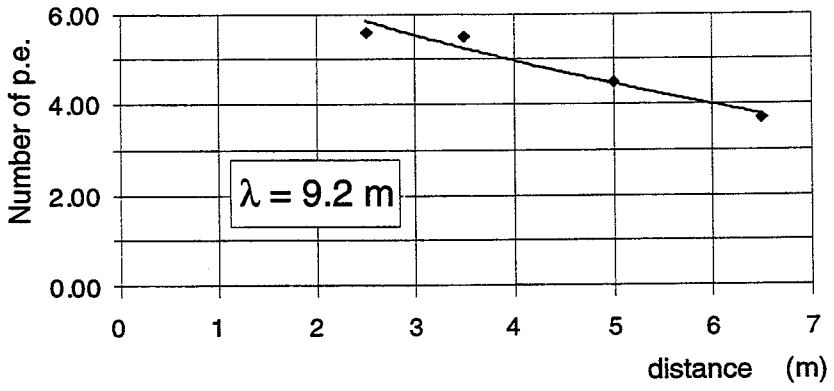

Figure 13: Number of photoelectrons vs. distance from photocathode for three cells made of polycarbonate profiles filled with liquid scintillator.

APPENDIX

A high-resolution tracking hodoscope based on capillary layers filled with liquid scintillator

A. Bay[a], L. Benussi[b], N. Bruski[c], S. Buontempo[c], C. Currat[a], N. D'Ambrosio[d], A.V. Ekimov[e], J.P. Fabre[f], V. Fanti[b], D. Frekers[d], A. Frenkel[g], S.V. Golovkin[e], V.N. Govorun[e], K. Harrison[g], P. Koppenburg[a], E.N. Kozarenko[h], I.E. Kreslo[g], B. Liberti[g], G. Martellotti[g], A.M. Medvedkov[e], M.R. Mondardini[i], G. Penso[g], W.P. Siegmund[j], V.G. Vasil'chenko[e], P. Vilain[b], G. Wilquet[b], K. Winter[i], H.J. Wörtche[d]

[a] *Université de Lausanne, Lausanne, Switzerland*
[b] *IIHE, ULB-VUB, Bruxelles, Belgium*
[c] *Università "Federico II" and INFN, Napoli, Italy*
[d] *Westfälische Wilhelms-Universität, Münster, Germany*
[e] *IHEP, Protvino, Russia*
[f] *CERN, Genève, Switzerland*
[g] *Università "La Sapienza" and INFN, Roma, Italy*
[h] *JINR, Dubna, Russia*
[i] *Humboldt-Universität, Berlin, Germany*
[j] *TaperVision, Inc., Pomfret, CT, USA*

Abstract

Results are given on tests of a high-resolution tracking hodoscope based on layers of 26-μm-bore glass capillaries filled with organic liquid scintillator (1-methylnaphthalene doped with R39). The detector prototype consisted of three 2-mm-thick parallel layers, with surface areas of 2.1×21 cm^2. The layers had a centre-to-centre spacing of 6 mm, and were read by an optoelectronic chain comprising two electrostatically focused image intensifiers and an Electron-Bombarded Charge-Coupled Device (EBCCD). Tracks of cosmic-ray particles were recorded and analysed. The observed hit density was 6.6 hits/mm for particles crossing the layers perpendicularly, at a distance of 1 cm from the capillaries' readout end, and 4.2 hits/mm for particles at a distance of 20 cm. A track segment reconstructed in a single layer had an rms residual of ~ 20 μm, and allowed determination of the track position in a neighbouring layer with a precision of ~ 170 μm. This latter value corresponded to an rms angular resolution per layer of about 30 mrad.

PACS: 29.40.Gx; 29.40.Mc; 42.79.Pw; 85.60.Gz
Keywords: Tracking and position-sensitive detectors; Scintillating fibres; Capillaries; Optoelectronics; Image intensifiers; EBCCD

(Submitted to Nuclear Instruments & Methods A)

1 Introduction

Tracking devices based on glass capillaries filled with liquid scintillator have been extensively studied over the past few years [1]. The principle of operation of the liquid-filled capillaries is the same as for glass and plastic scintillating fibres. Light is emitted when an ionizing particle traverses the liquid scintillator (core material) and a fraction of this light is trapped in the capillary through total internal reflection at the capillary walls (cladding material). The light that propagates in the capillaries forms an image of the particle track, and can be read using an optoelectronic chain. This typically consists of one or more image intensifiers coupled to a photosensitive Charge-Coupled Device (CCD) or to an Electron-Bombarded Charge-Coupled Device (EBCCD).

Glass and plastic scintillating fibres and liquid-filled capillaries (with diameters of 15–30 μm) have been assembled in coherent bundles, and give a spatial resolution of the order of tens of microns. Small-volume bundles (cross-section of 5×5 mm^2 and length of a few centimetres) have been investigated as active targets for studies of beauty production in a fixed-target environment [2]. In a more recent development, large-volume capillary bundles (cross-section of 2×2 cm^2 and length of up to 1.8 m) have been successfully tested [1] for use in neutrino experiments.

As an alternative to being assembled in bundles, capillaries and fibres can also be assembled in small-thickness layers. Such layers can be used to construct tracking devices with a geometry resembling that of a detector formed of silicon microstrip planes. Layers of large-diameter (0.5–1.0 mm) plastic scintillating fibres have been used in experiments UA2 [3, 4] and WA95-CHORUS [5] at CERN, and a beam-vertex detector based on one-fibre-thick layers of 200×200 μm^2 plastic fibres has been operated in experiment E917 [6] at the Brookhaven National Laboratory.

The light yield of specially prepared liquid scintillators [7–9] is sufficiently high that a capillary layer with a thickness of 1–2 mm and comprising capillaries of 20–30 μm bore will measure several points on the trajectory of a traversing particle. In contrast to a silicon microstrip plane, which measures a single track point per particle, a capillary layer will then record track segments, helping to reduce ambiguities in the reconstruction of high-multiplicity interactions. A method for track reconstruction in capillary layers, starting from track segments and using a Kalman-filter technique, has been developed [10] in a study of simulated events. For the situation considered in the present paper, the method has high efficiency if the average number of track points per layer is at least 6–7.

This paper presents results from tests of a detector prototype formed of three capillary layers. The layers had a thickness of 2 mm and consisted of capillaries having an inner diameter of 26 μm. Tracks of cosmic-ray particles were recorded, and have been used to evaluate the detector's spatial and angular resolution. Performance characteristics of capillary layers are compared with those of silicon microstrip planes.

The work summarized in this paper has been carried out in the framework of the CERN Research and Development Project RD46 [11].

2 Construction and filling of capillary layers

Each of the three layers in the detector prototype was composed of 10 elements, an individual element having square cross-section and comprising 4392 capillaries. These elements were drawn by TaperVision[1], and the layer assembly was performed at CERN.

[1] TaperVision Inc., Pomfret, CT 06258, USA.

A preform, obtained as a tube having a diameter of 36.5 mm and 1.5-mm-thick-walls of Schott[2] 8250 borosilicate glass (refractive index 1.49, density 2.28 g/cm^3, softening point 720°C), was drawn to produce capillaries with a diameter of 3.8 mm. These were stacked in groups of 61 to form mini-bundles of hexagonal cross-section (Fig 1). Rods of black glass were inserted in about a quarter of the interstices between capillaries, and acted as an extra-mural absorber (EMA) in the finished detector, suppressing crosstalk. Mini-bundles were drawn such that the distance between parallel sides was decreased from 30 mm to 2.3 mm.

Layer elements were assembled as arrays of 8 × 9 mini-bundles (Fig. 1). A final drawing stage then reduced the cross-section of a layer element from 18.3 × 18.5 mm^2 to approximately 2 × 2 mm^2. This drawing stage was performed at relatively low temperature, in order to limit surface tension's reduction of the packing fraction, defined as the ratio between the open area of a layer element and the element's total cross-section. After the final drawing stage, the capillaries' inner and outer diameters were respectively 26 μm and 32 μm, corresponding to a packing fraction of $\sim$ 67 %.

A layer was constructed from a set of 10 elements, glued together in a single row. No surrounding tube was placed about the elements, so that adjacent edges interlocked (Fig. 1). Each layer had transverse dimensions of 2×21 mm^2, including the small amount of glue, and was cut to a length of 21 cm.

Capillaries were filled with a liquid scintillator based on 1-methylnaphthalene (1MN, refractive index 1.62, density 1.0 g/cm^3) doped with 3 g/l of R39[3]. This scintillator emits in the green region, with peak emission at around 500 nm. The liquid scintillator was introduced into the layers through application of an argon overpressure, care being taken to avoid deterioration of the scintillator's light yield through contact with air. The filling procedure has been improved relative to that used previously [1], in that the filling apparatus is more compact and the filling time has been significantly reduced [12, 13].

Taking into account the total amounts of glass and liquid scintillator, the radiation length and interaction length for the layer material were respectively $X_0 = 25$ cm and $\lambda_I = 64$ cm.

3 Setup for tests

In the test setup, the three capillary layers were placed parallel to one another, with a centre-to-centre spacing of 6 mm, and formed a tracking hodoscope (Fig. 2). The performance of this hodoscope has been studied using cosmic-ray particles. The capillary layers, labelled L_1, L_2 and L_3, with L_1 uppermost, were read by an optoelectronic readout chain. This consisted of two image intensifiers followed by an EBCCD, all made by Geosphaera. A mechanical system allowed the layers to be pushed against the first image intensifier, so that the liquid scintillator contained in the capillaries came in direct contact with the entrance fibre-optic window of the readout chain.

The first image intensifier, which introduced a magnification of $m = 0.62$, had a multialkali photocathode of high quantum efficiency: about 20 % at $\sim$ 500 nm, the wavelength of maximum sensitivity. It was operated at a voltage of 15 kV and gave a gain of $\sim$ 25 photons per photon. The second image intensifier, of magnification $m = 1$, had an operating voltage of 7 kV and a gain of $\sim$ 8 photons per photon. The EBCCD [14] was essentially a zoomable image intensifier where a reversed, thinned CCD was mounted

[2]Schott Glas, 55122 Mainz, Germany.

[3]R39 is a trademark of the Geosphaera Research Centre, Moscow 117261, Russia.

in place of the phosphor screen. Electrons emitted at the photocathode were accelerated through 15 kV towards the CCD, which consisted of 1024 × 1024 pixels with areas of $13 \times 13\,\mu m^2$. In order that the layers' transverse dimensions should fit on the CCD, the voltage of the zoom electrode was set so as to magnify the image by a factor $m = 0.75$. Each capillary then occupied an area at the CCD corresponding to 1.2 pixels. The phosphor screens of the first and second image intensifiers had decay times of about 10 μs and 200 μs respectively. The slow response of the phosphors was adequate for the low-rate tests performed and provided an optical memory, allowing time for a trigger decision.

A cosmic-ray trigger was defined by a coincidence between two plastic scintillators measuring 2×2 cm^2. These were placed above and below the three capillary layers, at a variable distance d from their readout end. The trigger occurred about 150 ns after a physical event.

The EBCCD had no fast-clear facility, and the CCD chip was cleared by continuous readout at a pixel clock frequency of 10 MHz. When a trigger arrived, the clearing was interrupted and a gate pulse was applied to the EBCCD, enabling transmission of the image to the CCD. The light produced by the phosphor of the second image intensifier was integrated over a time of the order of 1 ms, and was then read in 110 ms by the acquisition system.

A reference grid, consisting of 20-μm-width transparent lines, etched at 2 mm intervals on the surface of a mirror, was positioned against the non-readout end of the capillary layers. The grid was used to check the overall magnification of the readout system, and to evaluate corrections for distortion. The mirror reflected incident light back towards the readout end.

4 Analysis and results

When the reference grid was illuminated from behind by an LED, the slight pincushion distortion introduced by the optoelectronic chain was seen in the image recorded by the CCD (Fig. 3a). The distortion was parameterised assuming that the magnification m of the chain varies with the distance R from the optical axis as $m(R) = m_0(1 + \alpha R + \beta R^2)$, where m_0 is the magnification on the axis. The parameters α and β were determined from a fit to the grid image and distortion effects were corrected for (Fig. 3b). The data for the reference grid were additionally used to define the region occupied at the CCD by each of the capillary layers.

Data for cosmic-ray particles were collected with the trigger counters at several distances from the capillaries' readout ends, with around 300 particle tracks recorded at each distance. During data taking, 8 background frames were read every 10 minutes (EBCCD gate closed), then the average pixel pulse height over the 8 frames was adopted as a measure of the dark-current background. Cosmic-ray events were recorded after background subtraction, with suppression of pixels having a pulse height below 30 ADC channels on a scale extending to 256. Track images for particles in triggered events (including some examples of interactions, not used in the subsequent analysis), were clearly seen in the three capillary layers (Fig. 4).

A track analysis was performed. Taking into consideration only the regions of the CCD corresponding to the capillary layers, clusters were obtained by grouping together adjacent pixels with pulse height above a threshold value set, after tuning, to 60 ADC channels. A cluster's centroid was calculated by averaging over the coordinates of the

Table 1: Root-mean-square track residuals for track fits relative to individual capillary layers and relative to all three layers, as a function of the distance d between track crossing point and readout surface.

	track residual (μm)			
d (cm)	layer L_1	layer L_2	layer L_3	all layers
1	30 ± 3	29 ± 3	26 ± 3	62 ± 2
3	25 ± 3	25 ± 3	21 ± 2	55 ± 2
5	22 ± 2	21 ± 2	20 ± 2	50 ± 1
9	21 ± 2	19 ± 2	21 ± 2	50 ± 1
15	22 ± 2	23 ± 2	21 ± 2	48 ± 1
20	22 ± 2	27 ± 3	23 ± 2	60 ± 2

cluster's pixels. In forming the average, pixel coordinates were corrected for the magnification and distortion of the readout system, and were weighted by the pixel pulse height. Sequences of approximately aligned clusters were identified, and straight lines were fitted to their centroids. These track fits were performed both for individual layers, with a requirement of at least 4 clusters in the layer considered, and for the three layers together, when a minimum of 15 clusters was required.

The gains of the optoelectronic chain and of the readout electronics were kept at relatively high values so as to avoid losing hits (electrons emitted at the photocathode of the first image intensifier and detected at the CCD). The high overall gain resulted in some merging of signals from hits that were close together, and so the number of hits per cluster used in the track reconstruction was sometimes greater than 1. The average number of hits per cluster has been estimated both through a statistical analysis of cluster pulse heights and through a visual examination of track images, and has been found to be ~ 1.6.

Hit densities for the three capillary layers decreased from 6.6 hits/mm to 4.2 hits/mm as the distance d between the trigger counters and the capillaries' readout ends was increased from 1 cm to 20 cm (Fig. 5). A single-exponential fit to the data on hit density as a function of d yields a light-attenuation length of 48 ± 9 cm, in good agreement with the short-distance attenuation measured for capillaries assembled in large-volume bundles [1].

Distributions of hit displacements from fitted tracks (track residuals) have been obtained both for track fits relative to a single capillary layer (Fig. 6a, 6b, 6c) and for the track fits relative to all three layers (Fig. 6d). Values for the root-mean-square (rms) track residual σ_{tr} have been calculated[4] and are reported in Table 1.

The spatial resolution achieved with an individual layer depends on physical effects (delta-ray production and Coulomb scattering), on the capillary geometry, on the layer uniformity, and on the resolution and distortion of the optoelectronic chain. The spatial resolution for the three layers together is additionally sensitive to inhomogeneities and misalignments of the layers. For $5 \text{ cm} \leq d \leq 20$ cm the individual layers were characterised by $\sigma_{tr} \simeq 20\,\mu$m, compared with $\sigma_{tr} \simeq 30\,\mu$m for capillaries in large-volume bundles [1], whereas the three layers together had $\sigma_{tr} \simeq 50\,\mu$m. For smaller d values ($d < 5$ cm), the diffuse crosstalk light encountered the EMA with lower probability and caused σ_{tr} to increase.

[4] In this paper, the root-mean-square of a distribution is evaluated as the full width at half maximum divided by $2\sqrt{2 \ln 2}$.

To estimate the angular resolution obtained with the detector prototype, tracks reconstructed in individual layers have been compared. For each event, tracks fitted in L_1 and tracks fitted in L_3 were extrapolated to L_2, and the coordinates x_1 and x_3 of their intersections with a reference axis, at the mid-height of L_2, were calculated. The coordinate x_2 at which the reference axis was crossed by the track fitted in L_2 was also determined. then the differences $\delta_{12} = x_1 - x_2$ and $\delta_{32} = x_3 - x_2$ were computed. The distributions of δ_{12} and δ_{32} for different distances d did not vary significantly. Their mean values were contained in an interval of $\sim \pm 50\,\mu$m, which is consistent with the layers being aligned to better than 0.5 mrad. Summed over all distances d, δ_{12} and δ_{32} had the distributions shown in Fig. 7, with rms values of $167 \pm 7\,\mu$m and $176 \pm 6\,\mu$m respectively. Recalling that the centre-to-centre spacing of the layers was 6 mm, these values imply that the rms angular resolution for a track reconstructed using a single capillary layer was about 30 mrad. For perfect layer geometry (no inhomogeneities), a Monte-Carlo calculation indicates that the angular resolution would be improved to $\sim$ 20 mrad.

5 Comparison between capillary layers and silicon microstrip planes

A detector based on capillary layers is in some ways similar to a detector formed of silicon microstrip planes. Both types of device consist of an arrangement of small-thickness modules, and both can be used as microvertex detectors for studies of the production and decay of short-lived particles, including charmed hadrons, beauty hadrons and tau leptons. Differences between the performance characteristics of the two kinds of modules can determine which is the more suitable for a given application. These differences are discussed below, with consideration of capillary layers of the type tested – layers having a thickness of 2 mm, corresponding to 8.1×10^{-3} radiation lengths – and silicon planes having a thickness of 300 μm, a value often used in practice [15–20] and equivalent to 3.2×10^{-3} radiation lengths.

A 2-mm-thick capillary layer records an average of about 10 hits along the track of a traversing charged particle at perpendicular incidence. In an experiment, track segments would be reconstructed in each individual layer and track segments from different layers would be matched for both position and direction. This can be of great help for pattern recognition, especially in the case of high-multiplicity events. Using a single layer, the rms track residual is $\sim$ 20 μm and, for the level of homogeneity currently achieved in layer construction, track angles are determined with an rms error of $\sim$ 30 mrad.

A 300-μm-thick silicon microstrip plane generally has a detection efficiency of between 0.90 and 0.98 [15–20]. For ideal efficiency, the number of measured points per traversing charged particle is 1 (or 2 for double-sided readout), so that the number of measured points per radiation length is lower than with capillaries by a factor of 4 (or 2 for double-sided readout). For pitch values between 10 μm and 60 μm, silicon microstrip planes give an rms track residual in the range 2-18 μm [15–20] (approximately $1/\sqrt{12}$ times the pitch), and so the point-measurement precision is better for silicon planes than for the capillary layers. However, the higher number of hits per radiation length using capillaries means that the two types of detector allow a similar precision in the determination of track parameters.

Capillary readout can be performed using optoelectronic components, which allow a high degree of multiplexing. For example, an optoelectronic chain based on one or more image intensifiers and a megapixel EBCCD allows readout of several capillary layers,

comprising 10^5-10^6 capillaries. Such a system has the advantage of a low cost per channel, but with the disadvantage that the readout time is long ($\sim$ 100 ms). Use of several CCDs operated in parallel, with multiple output registers, can significantly decrease the readout time. Alternative approaches, based on fast pixel photodetectors [12] or a high-speed gateable image pipeline [21], have also been studied for high rate experiments. A different situation is encountered with silicon detectors, where each microstrip requires a separate readout channel. This results in a relatively high cost per channel, but the readout is accomplished in a short time (of the order of tens of nanoseconds) with large numbers of channels read in parallel.

A detector based on capillary layers has a greater radiation resistance than a detector formed of silicon microstrip planes. Experience in collider experiments suggests that the degradation in the performance (efficiency and noise level) of a silicon microstrip plane becomes substantial after a radiation dose of a few tens of krad [16, 19]. In contrast, capillaries filled with an appropriate liquid scintillator are able to tolerate dose levels as high as 200 Mrad. Measurements [22] for capillaries filled using 1MN doped with R39 show that a dose of $\sim$ 200 Mrad decreases the scintillation yield by only about 30 % and reduces the attenuation length in the scintillator by a factor of 2–3 (not serious for the propagation distances relevant to capillary layers).

The surface area of a silicon microstrip plane is usually limited to not much greater than 5×5 cm^2. Capillary layers with detection surfaces considerably larger than this can be assembled by taking long capillaries (bundles of capillaries with lengths of 1.8 m have been successfully used for particle tracking [1]) and by gluing together a high number of layer elements.

Given the measured hit densities, capillary layers having a thickness smaller than 2 mm can also be constructed. A capillary layer with a depth of 1 mm would represent approximately the same amount of radiating material as a 300-μm-thick silicon plane, and would record an average of 5 hits per charged particle traversing the layer perpendicularly. This would result in limited angular information, but the particle-detection efficiency would remain high (probability of 99 % to record ≥ 1 hit).

6 Conclusions

A high-resolution tracking hodoscope comprising three layers of 26-μm-bore glass capillaries filled with organic liquid scintillator (1-MN doped with R39) has been tested. The layers had a thickness of 2 mm, a surface area of 2.1×21 cm^2, and a centre-to-centre spacing of 6 mm. Tracks of cosmic-ray particles have been recorded, with capillary readout by an optoelectronic chain consisting of two electrostatically focused image intensifiers and an EBCCD. The observed hit density was 6.6 hits/mm for particles crossing the layers at a distance of 1 cm from the capillaries' readout end, and 4.2 hits/mm for particles at a distance of 20 cm. A single-exponential fit to data on hit density as a function of distance gave the light-attenuation length in the capillaries to be 48 ± 9 cm. A track segment reconstructed in a single layer had an rms residual of $\sim$ 20 μm, and allowed determination of the track position in a neighbouring layer with a precision of $\sim$ 170 μm, corresponding to an rms angular resolution per layer of about 30 mrad. As compared with a typical 300-μm-thick silicon microstrip plane, the main characteristics of a capillary layer having a thickness of 1–2 mm (1.3–2.5 times the radiating material of the silicon plane) are: it records track segments (position and direction) rather than a single track point per particle, improving pattern recognition; it gives a higher number of hits

per radiation length; it has a slightly worse single-hit spatial resolution, but allows similar precision in track reconstruction; its readout time is long ($\sim$ 100 ms) with the most cost-effective readout schemes, but a much shorter readout time is also possible; it has a much higher radiation resistance (dose levels of up to 200 Mrad tolerated); it can have a larger detection surface. With these characteristics, capillary layers match requirements for track and vertex detectors in a wide variety of experiments.

Acknowledgements

This work has been carried out in the framework of the CERN Research and Development programme RD46. Finacial support was provided through the European Union's TMR Network Contract ERBFMRX-CT98-0196.

References

[1] P. Annis et al., Preprint CERN-EP/99-132 (1999), to be published in Nucl. Instr. and Meth. **A**, and references therein.

[2] C. Angelini et al., Nucl. Instr. and Meth. **A289** (1990) 342.

[3] R. E. Ansorge et al., Nucl. Instr. and Meth. **A273** (1988) 826.

[4] D.R. Wood, Nucl. Instr. and Meth. **A289** (1990) 331.

[5] P. Annis et al., Nucl. Instr. and Meth. **A409** (1998) 629.

[6] B.B. Beck et al., Nucl. Instr. and Meth. **A412** (1998) 191.

[7] V.G. Vasil'chenko et al., Instr. and Exp. Tech. **40** (1997) 175.

[8] S. Buontempo et al., Nucl. Instr. and Meth. **A425** (1999) 494.

[9] G.I. Britvich et al., Nucl. Instr. and Meth. **A425** (1999) 498.

[10] P. Koppenburg, Diploma Thesis, Université de Lausanne, 1997.

[11] R. van Dantzig et al., RD46 Proposal, CERN/LHCC 95-7, P60/LDRB, 1995.

[12] J. Konijn et al., Nucl. Instr. and Meth. **A418** (1998) 186.

[13] C. Currat, Thesis, Université de Lausanne, in preparation.

[14] S. Buontempo et al., Nucl. Instr. and Meth. **A413** (1998) 255.

[15] M. Adinolfi et al., Nucl. Instr. and Meth. **A329** (1993) 117.

[16] D. Amidei et al., Nucl. Instr. and Meth. **A350** (1994) 73.

[17] M. Acciarri et al., Nucl. Instr. and Meth. **A360** (1995) 103.

[18] V. Chabaud et al., Nucl. Instr. and Meth. **A368** (1996) 314.

[19] B. Mours et al., Nucl. Instr. and Meth. **A379** (1996) 101.

[20] S. Anderson et al., Nucl. Instr. and Meth. **A403** (1998) 326.

[21] A.G. Berkovski et al., Nucl. Instr. and Meth. **A380** (1996) 537.

[22] S.V. Golovkin et al., Nucl. Instr. and Meth. **A362** (1995) 283.

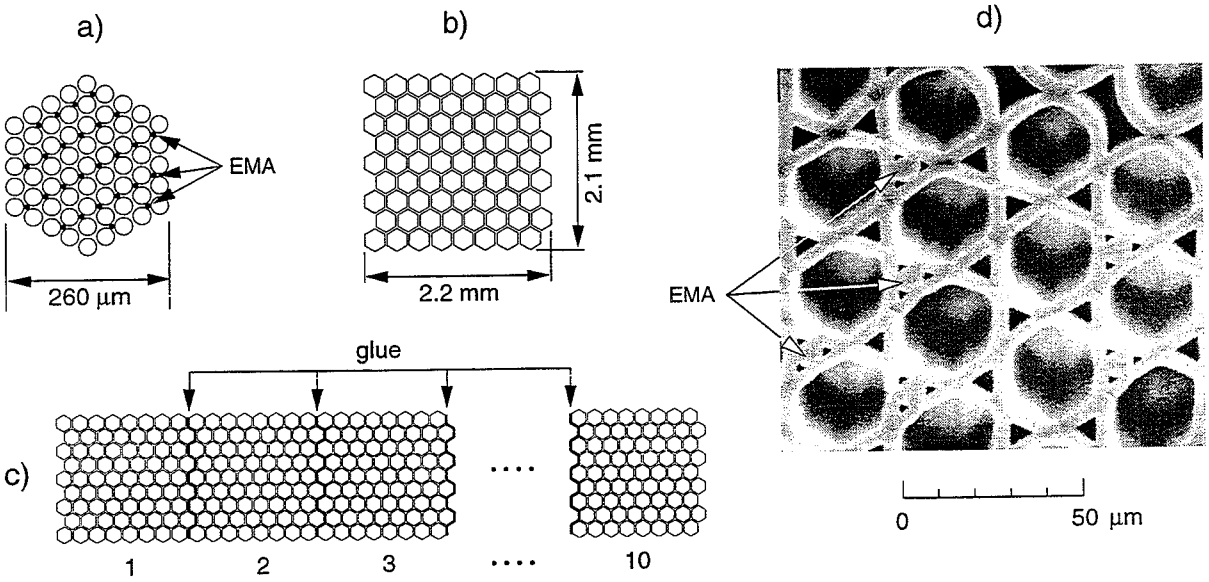

Figure 1: Cross-sectional views illustrating layer construction: a) a mini-bundle of 61 capillaries, with EMA present in a fraction of the inter-capillary spaces; b) a layer element, consisting of 8×9 mini-bundles; c) a capillary layer, formed by gluing together 10 elements; d) detail of a mini-bundle, photographed through an electron microscope.

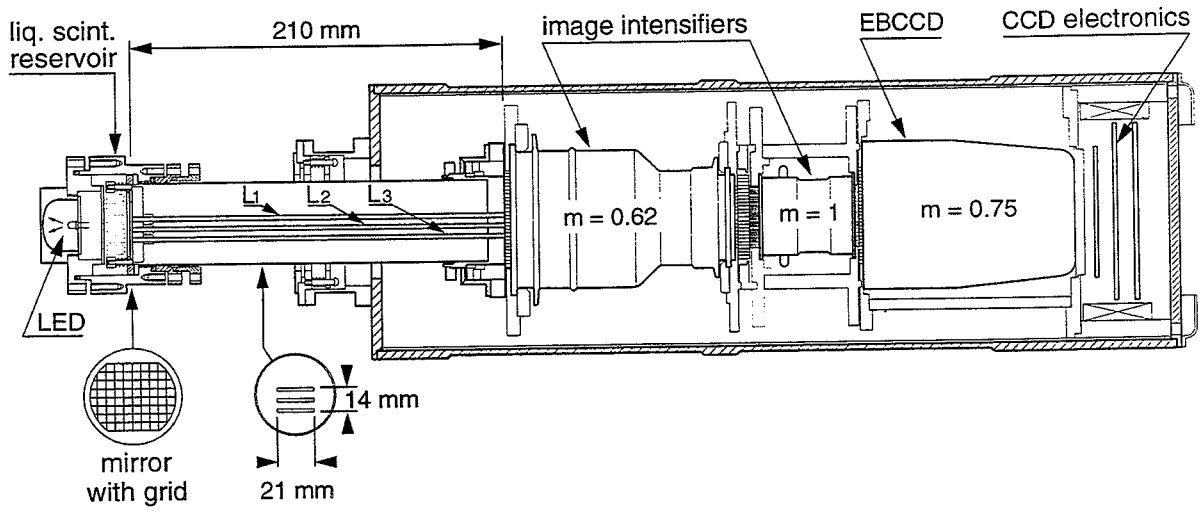

Figure 2: The three capillary layers (L_1, L_2, L_3) and their optoelectronic readout system, comprising two first-generation image intensifiers and a megapixel EBCCD. The magnification m of each component is indicated. A reference grid, placed at the non-readout end of the capillaries, could be illuminated from behind by an LED.

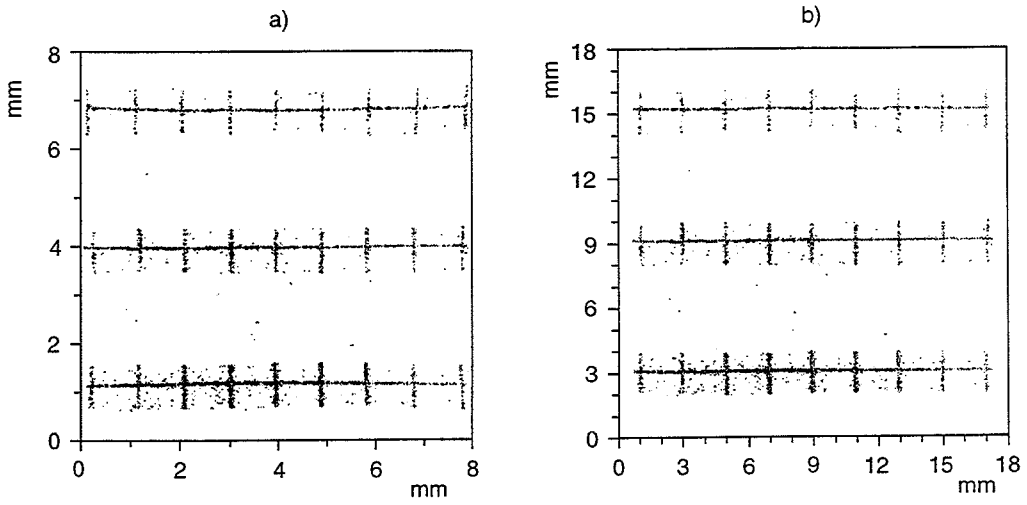

Figure 3: Removal of pincushion distortion introduced by the optoelectronic readout system: a) image of the reference grid as recorded by the EBCCD; b) outline of the grid reconstructed in the space of the capillary layers, after applying the corrections described in the text.

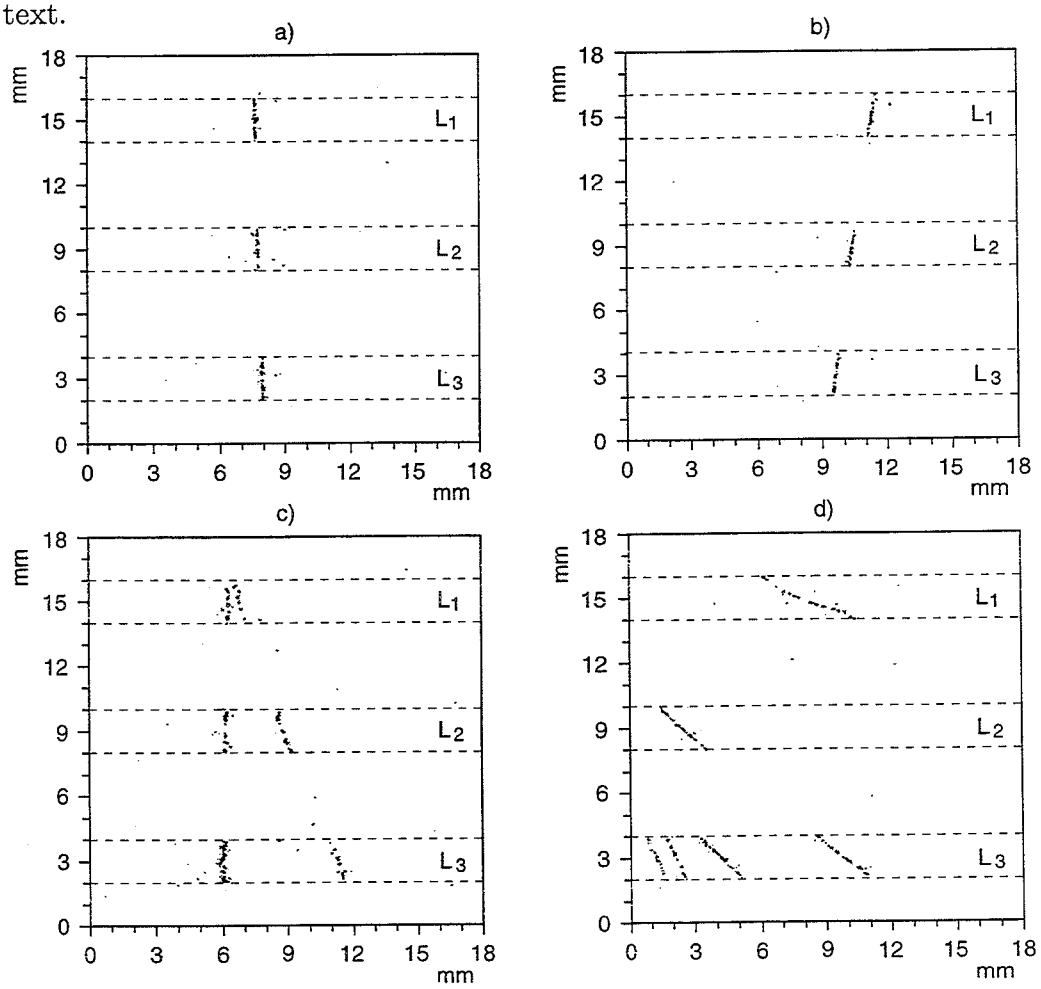

Figure 4: Examples of cosmic-ray events recorded in the capillary layers: a) and b) single-particle events; c) and d) interaction events, not used in the analysis. Dashed lines delimit the regions corresponding to the three layers L_1, L_2 and L_3.

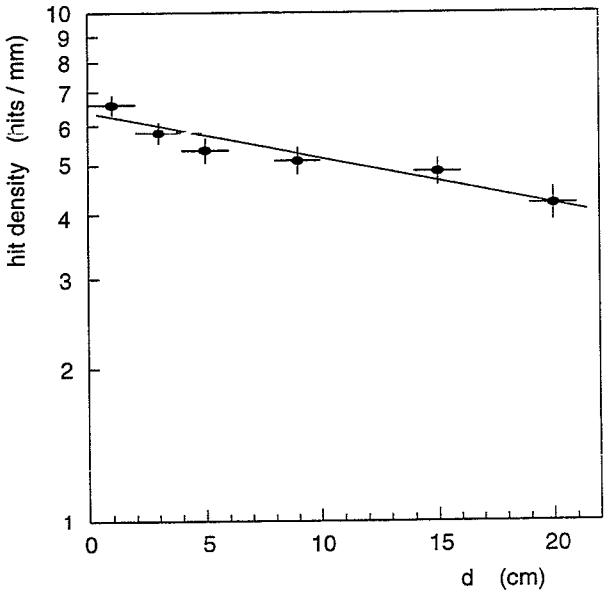

Figure 5: Measured hit density as a function of the track distance d from the readout end of the capillary layers. An exponential fit of the data points is shown, and corresponds to a light-attenuation length in the capillaries of 48 ± 9 cm.

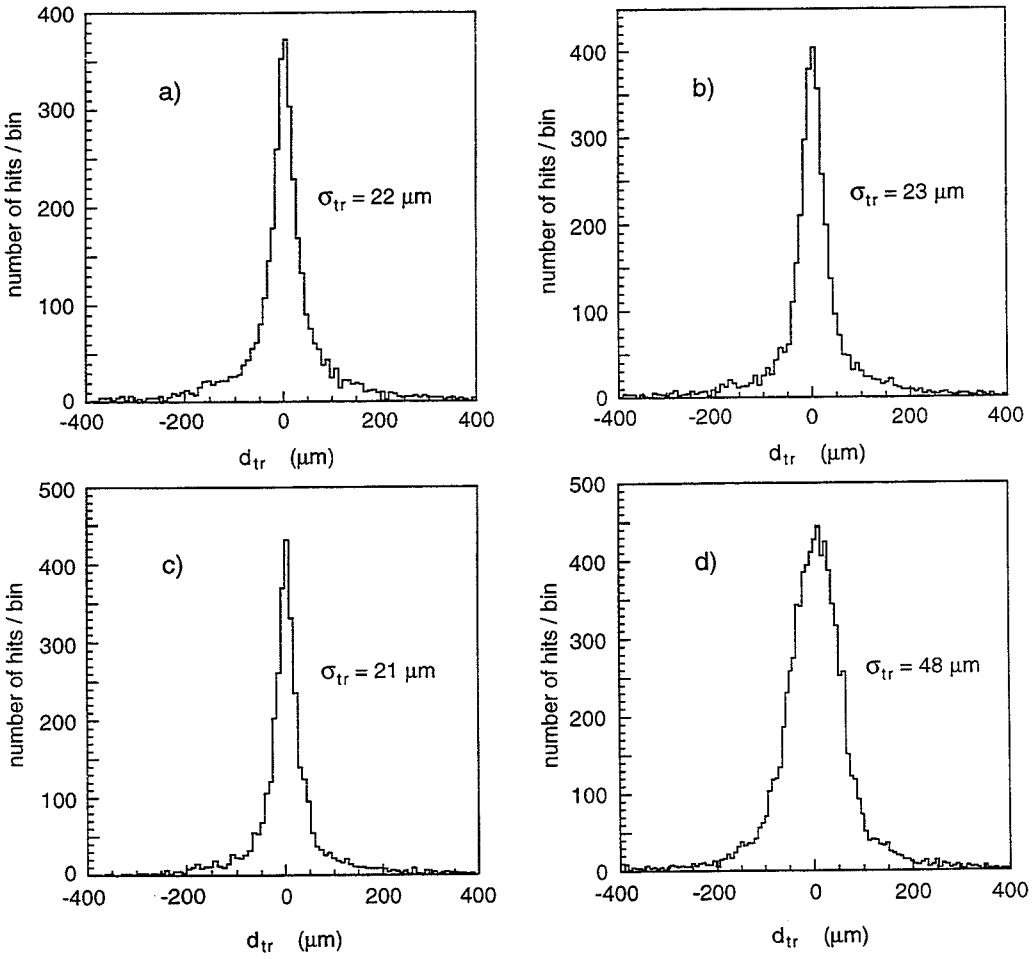

Figure 6: Distribution of track residual d_{tr} for tracks fitted in: a) layer L_1 only; b) layer L_2 only; c) layer L_3 only; d) all layers. Data shown are for tracks crossing the layers at a distance $d = 15$ cm from the readout surface. Similar distributions were obtained for other distances d, with root-mean-square values as reported in Table 1.

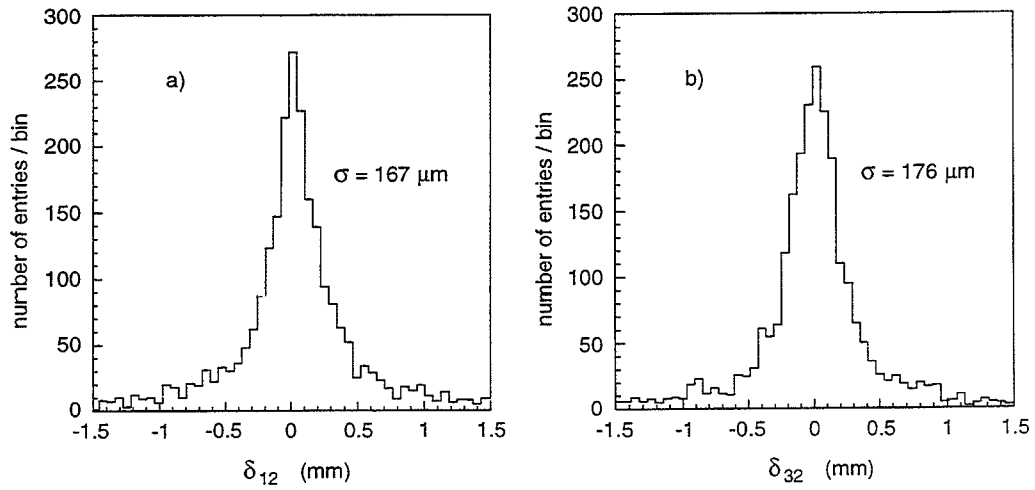

Figure 7: Distribution of: a) distance δ_{12} between track position measured in layer L_2 and position expected from extrapolation of track fitted in layer L_1; b) distance δ_{32} between track position measured in layer L_2 and position expected from extrapolation of track fitted in layer L_3. Data for tracks crossing the layers at different distances from the readout surface have been summed.